Journal of the Korean Electrochemical Society
Vol. 10, No. 3, 2007, 219-228

Determination of Adsorption Isotherms of Hydroxide at a Platinum Electrode Interface Using the Phase-Shift Method and Correlation Constants

Jin Y. Chun and Jang H. Chun†*

School of Chemical and Biological Engineering, Seoul National University, Seoul 151-744, Republic of Korea
†Department of Electronic Engineering, Kwangwoon University, Seoul 139-701, Republic of Korea

(Received July 25, 2007 : Accepted August 1, 2007)

Abstract : The phase-shift method and correlation constants, i.e., the electrochemical impedance spectroscopy (EIS) techniques for studying linear relationships between the behaviors ($-\varphi$ vs. E) of the phase shift ($0^o \leq -\varphi \leq 90^o$) for the optimum intermediate frequency and those (θ vs. E) of the fractional surface coverage ($1 \geq \theta \geq 0$), have been proposed and verified to determine the Langmuir, Frumkin, and Temkin adsorption isotherms (θ vs. E) of H for the cathodic H_2 evolution reaction (HER) at noble and transition-metal/aqueous solution interfaces. At the Pt/0.1 M KOH aqueous solution interface, the Langmuir, Frumkin, and Temkin adsorption isotherms (θ vs. E), equilibrium constants ($K = 5.6 \times 10^{-10}$ mol^{-1} at $0 \leq \theta < 0.81$, $K = 5.6 \times 10^{-9}\exp(-4.6\theta)$ mol^{-1} at $0.2 < \theta < 0.8$, and $K = 5.6 \times 10^{-10}\exp(-12\theta)$ mol^{-1} at $0.919 < \theta \leq 1$), interaction parameters ($g = 4.6$ for the Temkin and $g = 12$ for the Frumkin adsorption isotherm), rates of change of the standard free energy ($r = 11.4$ kJ mol^{-1} for $g = 4.6$ and $r = 29.8$ kJ mol^{-1} for $g = 12$), and standard free energies ($\Delta G_{ads}^0 = 52.8$ kJ mol^{-1} at $0 \leq \theta < 0.81$, $49.4 < \Delta G_\theta^0 < 56.2$ kJ mol^{-1} at $0.2 < \theta < 0.8$, and $80.1 < \Delta G_\theta^0 \leq 82.5$ kJ mol^{-1} at $0.919 < \theta \leq 1$) of OH for the anodic O_2 evolution reaction (OER) are also determined using the phase-shift method and correlation constants. The adsorption of OH transits from the Langmuir to the Frumkin adsorption isotherm (θ vs. E), and vice versa, depending on the electrode potential (E) or the fractional surface coverage (θ). At the intermediate values of θ, i.e., $0.2 < \theta < 0.8$, the Temkin adsorption isotherm (θ vs. E) correlating with the Langmuir or the Frumkin adsorption isotherm (θ vs. E), and vice versa, is readily determined using the correlation constants. The phase-shift method and correlation constants are accurate and reliable techniques to determine the adsorption isotherms and related electrode kinetic and thermodynamic parameters. They are useful and effective ways to study the adsorptions of intermediates (H, OH) for the sequential reactions (HER, OER) at the interfaces.

Keywords : Phase-shift method, Adsorption isotherms, Hydroxide adsorption, Pt electrode, Electrochemical impedance spectroscopy (EIS).

1. Introduction

To obtain an environmentally clean energy source, i.e., hydrogen energy, fuel cell, etc., many experimental methods have been used to study the cathodic H_2 evolution reaction (HER) and anodic O_2 evolution reaction (OER) at electrode/aqueous solution interfaces. The adsorptions of H and OH have been extensively studied to understand the kinetics and mechanisms of the cathodic HER and anodic OER at the interfaces.[1-8] Although the Langmuir, Frumkin, and Temkin adsorption isotherms may be regarded classical models and theories in electrochemistry, surface chemistry and physics, etc., they are useful and effective ways to study the adsorptions of intermediates (H, OH) for the sequential reactions (HER, OER) at the interfaces.

Linear relationships between the behaviors ($-\varphi$ vs. E) of the phase shift ($0^o \leq -\varphi \leq 90^o$) for the optimum intermediate frequency and those (θ vs. E) of the fractional surface coverage ($1 \geq \theta \geq 0$) of H for the cathodic HER have been experimentally verified at noble and transition-metal/aqueous solution interfaces.[9-26] The phase-shift method is an electrochemical impedance spectroscopy (EIS) technique for studying the linear relationships between $-\varphi$ vs. E and θ vs. E. At first glance, it seems that there are no linear relationships between the phase-shift profiles ($-\varphi$ vs. E) for the optimum intermediate frequency and the Langmuir, Frumkin, and Temkin adsorption isotherms (θ vs. E). The arguments on the phase-shift method in the Comments[27,28] are attributed to the misunderstandings and confusions on the newly defined equivalent circuit elements for the phase-shift method, the simplified equivalent circuit for the optimum intermediate frequency response, the linear relationship between the behavior ($-\varphi$ vs. E) of the phase shift ($0^o \leq -\varphi \leq 90^o$) for the optimum intermediate frequency and that (θ vs. E) of the fractional surface coverage ($1 \geq \theta \geq 0$), etc. In addition, the lack of a single equation for $-\varphi$ vs. θ as a function of potential (E) and frequency (f) and the overlook of a unique nature and combination of the faradaic resistance (R_ϕ) and adsorption pseudocapacitance (C_ϕ) in the Comment[28] result in a wrong conclusion. However, on the contrary, the

*E-mail: jhchun@kw.ac.kr

Comments[27,28] verify the validity and effectiveness of the phase-shift method. It is clearly explained, stated, and summarized in the Responses[29,30] and references.[25,26] Correspondingly, it appears that the phase-shift method is an accurate and reliable technique to determine the Langmuir, Frumkin, and Temkin adsorption isotherms (θ vs. *E*) and related electrode kinetic and thermodynamic parameters at these interfaces.

In practice, the theoretical derivation or the numerical calculation of a single equation for $-\varphi$ vs. θ as a function of *E* and *f* is impossible due to the superposition of various effects, i.e., the relaxation time effect, the surface absorption and diffusion processes, the inhomogeneous and lateral interaction effects, the specific adsorption effect, etc., which are inevitable at these interfaces. Thus, there is a technological need for a fast, simple, and effective method to determine the Langmuir, Frumkin, and Temkin adsorption isotherms (θ vs. *E*) of intermediates (H, OH) for the sequential reactions (HER, OER). This is the reason why the phase-shift method is necessary and useful.

In general, the anodic OER at Pt group metal/alkaline aqueous solution interfaces can be expressed as follows[31-33]

$$M + OH^- \underset{k_{-1}}{\overset{k_1}{\rightleftarrows}} MOH_{ads} + e, \quad (1)$$

$$MOH_{ads} + OH^- \xrightarrow{k_2} MO_{ads} + H_2O + e, \quad (2)$$

$$2MO_{ads} \xrightarrow{k} 2M + O_2, \quad (3)$$

where M is an electrode surface atom, e is an electron, OH_{ads} is the adsorbed hydroxide on the M, and O_{ads} is the adsorbed oxygen on the M. For the anodic OER, k_1, k_{-1}, and k_2 are the electrochemical rate constants and k_3 is the chemical rate constant. Equations (1), (2), and (3) are known as the hydroxide ion (OH^-) discharge, electrochemical desorption, and recombination reactions, respectively. For the adsorption of OH, i.e., the hydroxide ion (OH^-) discharge reaction described in Eq. (1), the reverse reactions corresponding to the electrochemical desorption and recombination reactions described in Eqs. (2) and (3) are not considered.

In this paper, we represent the Langmuir, Frumkin, and Temkin adsorption isotherms (θ vs. *E*) of OH for the anodic OER at a Pt/0.1 M KOH aqueous solution interface using the phase-shift method and correlation constants. The Temkin adsorption isotherm (θ vs. *E*) correlating with the Langmuir or the Frumkin adsorption isotherm (θ vs. *E*) is readily determined using the correlation constants. The three Langmuir, Frumkin, and Temkn adsorption isotherms (θ vs. *E*) of OH at the interface have never been reported elsewhere. Note that they cannot be readily determined or distinguished using the conventional methods.[1-8] It appears that the phase-shift method and correlation constants are useful and effective ways to study the adsorptions of intermediates (H, OH) for the sequential reactions (HER, OER) at the interfaces.

2. Experimental

2.1. Preparations

Taking into account the OH^- concentration and the effect of pH,[34] an alkaline aqueous solution was prepared from KOH (Alfa Aesar, reagent grade) with purified water (resistivity : > 18 MΩ cm) obtained from a Millipore system. The 0.1 M KOH aqueous solution (pH 12.99, i.e., pOH 1.01) was deaerated with 99.999% purified nitrogen gas for 20 min before the experiments.

A standard three-electrode configuration was employed using a saturated calomel electrode (SCE) reference electrode and a Pt wire (Johnson Matthey, purity : 99.998%, 1 mm diameter, estimated surface area : ~0.85 cm^2) working electrode. The Pt working electrode was prepared by flame cleaning and then quenched and cooled in Millipore Milli-Q water and in air, sequentially. A Pt wire (Johnson Matthey, purity: 99.95%, 1.5 mm diameter) was used as the counter electrode. The working and counter electrodes were separated by ca. 4 cm in the same compartment of a Pyrex cell using Teflon holders.

2.2. Measurements

A cyclic voltammetry (CV) technique was used to achieve a steady state at the Pt/0.1 M KOH aqueous solution interface. The CV experiments were conducted for 20 cycles, a scan rate of 200 mV/s, and a scan potential of 0 to 1.40 V vs. SCE. An electrochemical impedance spectroscopy (EIS) technique was used to study the relation between the phase-shift profile ($-\varphi$ vs. *E*) for the optimum intermediate frequency and the corresponding adsorption isotherm (θ vs. *E*). The EIS experiments were conducted at a frequency of 10^4 to 1 Hz for an intermediate frequency response, frequency of 10^5 to 10^2 Hz for a high frequency response, frequency of 1 to 10^{-4} Hz for a low frequency response, single sine wave, ac amplitude of 5 mV, and dc potential of 0 to 1.150 V vs. SCE.

The CV experiments were performed using an EG&G PAR Model 273A potentiostat controlled with the PAR Model 270 software package. The EIS experiments were performed using the same apparatus in conjunction with a Schlumberger SI 1255 HF Frequency Response Analyzer controlled with the PAR Model 398 software package. To obtain comparable and reproducible results, all measurements were carried out using the same preparations, procedures, and conditions at room temperature. The international sign convention is used, i.e., anodic currents and lagged phase shifts or angles are taken as positive and negative, respectively. Taking into account the adsorption of OH, all potentials are given in the saturated calomel electrode (SCE) scale.

3. Results and Discussion

3.1. Phase-shift profile for the optimum intermediate frequency response

The adsorption of OH for the anodic OER at the Pt/0.1 M KOH aqueous solution interface can be expressed as the equivalent circuit shown in Fig. 1(a).[35-37] In Fig. 1(a), R_S is the aqueous solution resistance, R_ϕ is the faradaic resistance for the adsorption of OH, i.e., the hydroxide ion (OH^-) discharge reaction described in Eq. (1), R_R is the faradaic resistance for the recombination reaction, C_ϕ is the pseudocapacitance for the adsorption of OH, i.e., the hydroxide

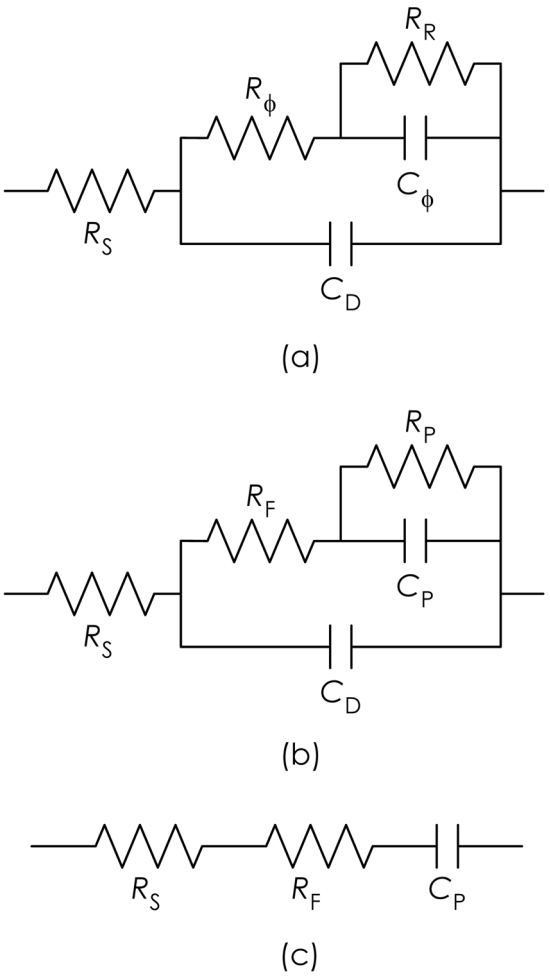

Fig. 1. (a) Equivalent circuit at the interface, (b) newly defined equivalent circuit at the interface, and (c) simplified equivalent circuit for the intermediate frequency response at the interface.

ion (OH^-) discharge reaction described in Eq. (1), and C_D is the double-layer capacitance. The faradaic resistance (R_ϕ) is associated with finite rates of charging the pseudocapacitance (C_ϕ). Note that both R_ϕ and C_ϕ are not constant but dependent on E and θ and cannot be measured at the interface.

A unique nature of C_ϕ attaining a maximum value at θ = 0.5, decreasing symmetrically with E at other values of θ, approaching a minimum value at θ ≈ 0 and 1, and attaining a minimum value at θ = 0 and 1 is well known in interfacial electrochemistry, electrode kinetics, and EIS.[2-8,35-37] A unique nature of R_ϕ is similar to that of C_ϕ. This implies that the adsorption of OH can be expressed as the unique nature and combination of R_ϕ and C_ϕ vs. E, i.e., a linear relationship between −φ vs. E and θ vs. E. In other words, the adsorption of OH can be accurately expressed in terms of the rates of change of −φ vs. E and θ vs. E. The rate of change of −φ vs. E, i.e., $\Delta(-\varphi)/\Delta E$ or $d(-\varphi)/dE$, corresponds to that of θ vs. E, i.e., $\Delta\theta/\Delta E$ or $d\theta/dE$, and vice versa. Both $\Delta(-\varphi)/\Delta E$ or $d(-\varphi)/dE$ and $\Delta\theta/\Delta E$ or $d\theta/dE$ are maximized at θ ≈ 0.5, decrease symmetrically with E at other values of θ, and are minimized at θ ≈ 0 and 1 (see Table 1 and Fig. 6). Note that this is a unique feature of the Langmuir and Frumkin adsorption isotherms (θ vs. E). The Langmuir and Frumkin adsorption isotherms (θ vs. E) can be distinctively determined based on the linear relationship between −φ vs. E and θ vs. E. Because the interaction parameter (g) for the Frumkin adsorption isotherm (θ vs. E) is readily determined or distinguished referred to the Langmuir adsorption isotherm (θ vs. E), i.e., g = 0 (see Fig. 8). This is discussed in more detail in the section on the Langmuir, Frumkin, and Temkin adsorption isotherms. Consequently, one can interpret that the behavior (−φ vs. E) of the phase shift ($0^o \le -\varphi \le 90^o$) for the optimum intermediate frequency corresponds to that (θ vs. E) of the fractional surface coverage ($1 \ge \theta \ge 0$) and vice versa (see Figs. 6-10).

Taking into account the superposition of various effects at the interface, i.e., the relaxation time effect, the surface absorption and diffusion processes, the inhomogeneous and lateral interaction effects, the specific adsorption effect, etc., which are inevitable under the EIS experiments, we define the equivalent circuit elements shown in Fig. 1(b). R_S is the aqueous solution resistance, R_F is the equivalent resistance due to the faradaic resistance (R_ϕ) and superposition of various effects, R_P is the equivalent resistance due to the faradaic resistance (R_R) and superposition of various effects, C_P is the equivalent capacitance due to the pseudocapacitance (C_ϕ) and superposition of various effects, and C_D is the double-layer capacitance. Note that both R_F and C_P are not constant but dependent on E and θ and can be measured at the interface.

The frequency responses of the equivalent circuit for all frequencies shown in Fig. 1(b) are essential for verifying the unique nature and combination of R_ϕ and C_ϕ vs. E, i.e., the linear relationship between −φ vs. E and θ vs. E. At very low frequencies, the equivalent circuit for all frequencies shown in Fig. 1(b) can be expressed as a series circuit of R_S, R_F, and R_P. Note that the values of $1/\omega C_P$ are much greater than those of R_P, where ω is the angular frequency. At very high frequencies, the equivalent circuit for all frequencies shown in Fig. 1(b) can be expressed as a series circuit of R_S and C_D. Note that the values of R_F are much greater than those of $1/\omega C_D$. At intermediate frequencies and for a wide range of θ, the equivalent circuit for all frequencies shown in Fig. 1(b) can be simplified as the series circuit of R_S, R_F, and C_P shown in Fig. 1(c). Note that the simplified equivalent circuit shown in Fig. 1(c) is not for the change of the anodic OER itself but only the intermediate frequency response.

The impedance (Z) of the simplified equivalent circuit shown in Fig. 1(c) and the corresponding lagged phase shift (−φ) or angle are given by

$$Z = (R_S + R_F) - j/\omega C_P, \quad (4)$$

$$-\varphi = \tan^{-1}[1/\omega(R_S + R_F)C_P], \quad (5)$$

$$R_F >> R_S \text{ and } C_P >> C_D \text{ (for a wide range of } \theta), \quad R_P >> 1/\omega C_P,\ R_F \propto R_\phi, \text{ and } C_P \propto C_\phi, \quad (6)$$

where j is an operator and is equal to the square root of −1, i.e., $j^2 = -1$, ω (= $2\pi f$) is the angular frequency, f is the inter-

Table 1. Measured values of the equivalent circuit elements for the intermediate frequency (1.0 Hz) and the estimated fractional surface coverage (θ) of OH at the Pt/0.1 M KOH aqueous solution interface.

E (V vs. SCE)	$R_S + R_F$ (Ω cm^2)	C_P [a] (μF cm^{-2})	$-\varphi$ [b] (deg)	$-\varphi$ (deg)	θ [c] ($0 \leq \theta \leq 1$)
0.450	518.2	29.3	84.6	84.6	≈ 0
0.475	525.1	29.4	84.5	84.5	0.001
0.500	552.0	29.8	84.1	84.1	0.006
0.525	635.3	30.5	83.1	83.1	0.018
0.550	935.9	31.9	79.4	79.4	0.062
0.575	1716.2	36.7	68.4	68.4	0.193
0.600	2433.6	60.6	47.2	47.2	0.446
0.625	1938.9	159.2	27.3	27.3	0.683
0.650	1290.3	397.1	17.3	17.3	0.802
0.675 [d]	957.1	698.5	13.4	13.4	0.849
0.700 [d]	822.4	867.4	12.6	12.6	0.858
0.725 [d]	772.5	895.8	13.0	13.0	0.853
0.750 [d]	694.1	1032.0	12.5	12.5	0.859
0.775 [d]	569.8	1423.5	11.1	11.1	0.876
0.800 [d]	453.6	2018.8	9.9	9.9	0.890
0.825 [d]	349.9	2818.8	9.2	9.2	0.899
0.850 [d]	284.8	3344.7	9.5	9.5	0.895
0.875 [d]	244.6	3641.2	10.1	10.1	0.888
0.900 [d]	212.7	3997.6	10.6	10.6	0.882
0.925 [d]	186.1	4896.5	9.9	9.9	0.890
0.950	145.2	8312.9	7.5	7.5	0.919
0.975	104.3	18223.5	4.8	4.8	0.951
1.000	73.6	41764.7	3.0	3.0	0.973
1.025	53.7	91105.9	1.9	1.9	0.986
1.050	41.8	149529.4	1.5	1.5	0.990
1.075	34.5	281529.4	0.9	0.9	0.998
1.100	30.1	429647.1	0.7	0.7	≈ 1

[a] C_P practically includes C_D ($C_P >> C_D$ except for low values of θ).
[b] Calculated using R_S, R_F, C_P, and Eq. (5).
[c] Estimated using the measured phase shift ($-\varphi$).
[d] Transition region between the Langmuir and Frumkin adsorption isotherms (θ vs. E).

mediate frequency, and θ ($0 \leq \theta \leq 1$) is the fractional surface coverage of OH. In Eq. (5), $-\varphi$ is substantially determined by the combination of R_F and C_P. Note that the measured values of R_F and C_P for the intermediate frequency (1 Hz) are much greater than those of R_S and C_D, i.e., ~10.4 Ω cm^2 and ~7.6 μF cm^{-2}, respectively (see Table 1).

Figs. 2(a) and (b) show the profiles of the measured R_F and C_P vs. E for the intermediate frequency (1 Hz) at the Pt/0.1 M KOH aqueous solution interface, respectively. Fig. 2(a) shows that R_F is smaller than R_ϕ, because the right side of the profile (R_F vs. E) is lower than the left side of the profile. Fig. 2(b) shows that C_P is greater than C_ϕ, because the profile (C_P vs. E) increases from the left side to the right side, i.e., towards more positive potentials. This is attributed to the reciprocal property of R_F and C_P due to the superposition of various effects at the interface. Because the nature of a resistance is inversely proportional to the concentration of charged species (OH^-) due to the superposition of various effects, but the nature of a capacitance is proportional to the concentration of charged species (OH^-) due to the superposition of various effects. Fig. 2(b) also shows that C_P increases rapidly beyond the peak potential, i.e., ca. 0.611 V vs. SCE, of the equivalent

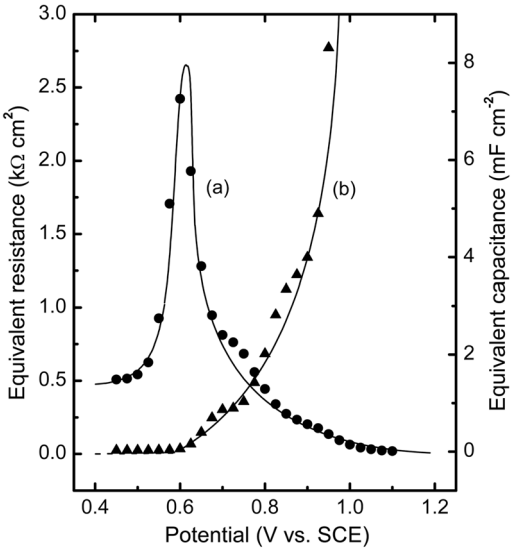

Fig. 2. Profiles of the measured equivalent circuit elements (R_F, C_P) vs. E for the intermediate frequency (1 Hz) at the Pt/0.1 M KOH aqueous solution interface : (a) Equivalent resistance profile (R_F vs. E) and (b) equivalent capacitance profile (C_P vs. E). Note that the transition occurs at ca. 0.675 to 0.925 V vs. SCE (see Table 1).

resistance profile (R_F vs. E). It is understood that both R_ϕ and C_ϕ have maximum values at ca. 0.611 V vs. SCE, i.e., $\theta = 0.5$ (see Table 1 and Fig. 6). However, note that the equivalent resistance profile (R_F vs. E) shown in Fig. 2(a) has a peak. But, the equivalent capacitance profile (C_P vs. E) shown in Fig. 2(b) has no peak. This is also attributed to the reciprocal property of R_F and C_P due to the superposition of various effects at the interface. Consequently, one can interpret that the superposition of various effects on R_F and C_P in Eq. (5) is cancelled out or compensated together and so the combination of R_F and C_P is equivalent to that of R_ϕ and C_ϕ. The behavior ($-\varphi$ vs. E) of the phase shift ($0^o \leq -\varphi \leq 90^o$) for the optimum intermediate frequency corresponds to that (θ vs. E) of the fractional surface coverage ($1 \geq \theta \geq 0$) and vice versa (see Figs. 6-10).

Fig. 3 compares the Nyquist impedance plots (Z_{IM} vs. Z_{RE}) for the different electrode potentials (E) at the Pt/0.1 M KOH aqueous solution interface. In this figure, Z_{IM} and Z_{RE} refer to the imaginary and real parts of the impedance (Z), respectively. The values of ω ($= 2\pi f$), which are not shown in Fig. 3, increase from the outside, i.e., 1 Hz, to the origin of the Z_{IM} and Z_{RE} axes, i.e., 10^4 Hz. Note that Z_{IM} and Z_{RE} are not constant but dependent on E and θ, i.e., the adsorption of OH. The Nyquist impedance plots (Z_{IM} vs. Z_{RE}) shown in Fig. 3 correspond to the phase-shift curves ($-\varphi$ vs. log f) shown in Fig. 4 and vice versa.

Fig. 4 compares the phase-shift curves ($-\varphi$ vs. log f) for the different electrode potentials (E), i.e., 0.450 to 1.100 V vs. SCE (see Table 1), at the Pt/0.1 M KOH aqueous solution interface. The intermediate frequency, i.e., a vertical solid line (1 Hz) on the phase-shift curves ($-\varphi$ vs. log f) shown in Fig. 4, can be set as the optimum intermediate frequency for the phase-shift profile ($-\varphi$ vs. E). Note that the optimum intermediate frequency (1 Hz) can cover a wide range of $-\varphi$, i.e., $84.6^o \geq -\varphi \geq 0.7^o$, on the phase-shift curves ($-\varphi$ vs. log f) shown in Fig. 4. At the optimum intermediate frequency (1 Hz), the rates of change of $-\varphi$ vs. E and θ vs. E, i.e., $\Delta(-\varphi)/\Delta E$ or $d(-\varphi)/dE$ and $\Delta\theta/\Delta E$ or $d\theta/dE$, obey a Gaussian profile (see Fig. 6). This implies that the phase-shift profile ($-\varphi$ vs. E) for the optimum intermediate frequency (1 Hz) can be interpreted as the corresponding

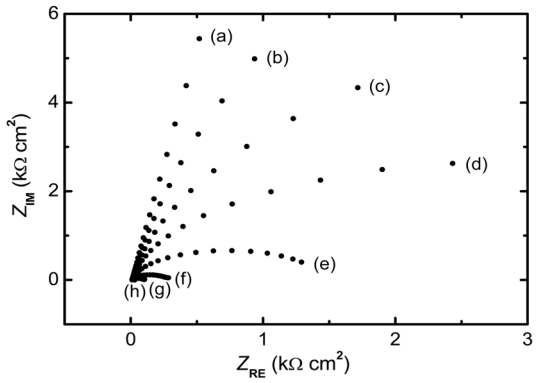

Fig. 3. Comparison of the Nyquist impedance plots (Z_{IM} vs. Z_{RE}) at the Pt/0.1 M KOH aqueous solution interface. Single sine wave; frequency : 10^4 to 1 Hz; ac amplitude : 5 mV; dc potential : (a) 0.450 V, (b) 0.550 V, (c) 0.575 V, (d) 0.600 V, (e) 0.650 V, (f) 0.850 V, (g) 0.975 V, and (h) 1.100 V vs. SCE.

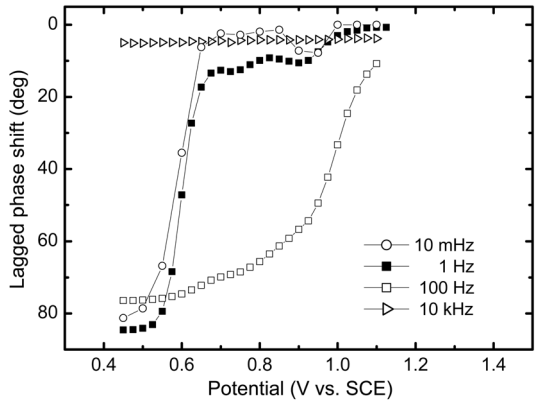

Fig. 5. Comparison of the phase-shift profiles ($-\varphi$ vs. E) for four different frequencies at the Pt/0.1 M KOH aqueous solution interface.

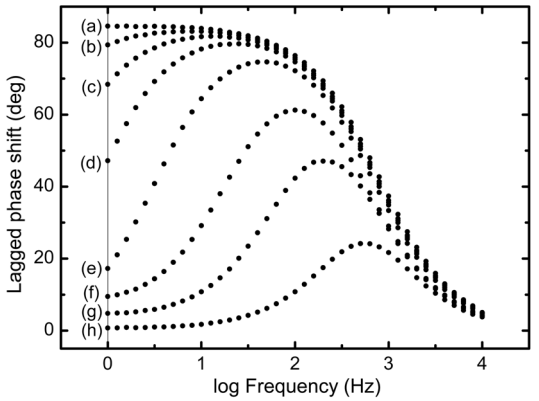

Fig. 4. Comparison of the phase-shift curves ($-\varphi$ vs. log f) at the Pt/0.1 M KOH aqueous solution interface. Vertical solid line : 1 Hz; dc potential: (a) 0.450 V, (b) 0.550 V, (c) 0.575 V, (d) 0.600 V, (e) 0.650 V, (f) 0.850 V, (g) 0.975 V, and (h) 1.100 V vs. SCE.

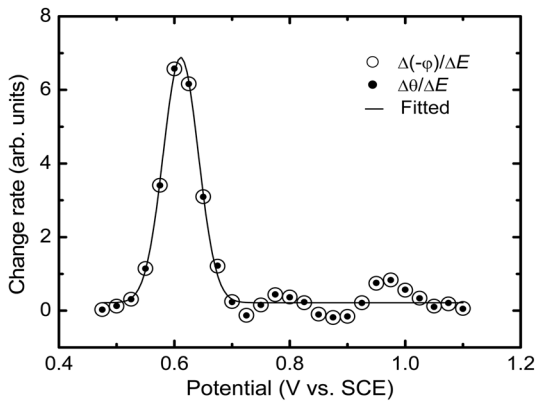

Fig. 6. Comparison of the rates of change of $-\varphi$ vs. E and θ vs. E for the adsorption of OH at the Pt/0.1 M KOH aqueous solution interface. Note that the transition occurs at ca. 0.675 to 0.925 V vs. SCE (see Table 1).

adsorption isotherm (θ vs. *E*) at the interface (see Figs. 7 and 8). At the maximum lagged phase shift for the optimum intermediate frequency (1 Hz) shown in Fig. 4(a), i.e., 84.6° at 0.450 V vs. SCE, it appears that the adsorption of OH and superposition of various effects are minimized. In other words, θ can be set to zero. At θ ≈ 0, $1/\omega C_P$ is much greater than $(R_S + R_F)$ (see Table 1 and Fig. 3(a)). In Eqs. (4)-(6), *Z* is substantially determined by $1/\omega C_P$, i.e., Z_{IM}, and so −φ has a maximum value of ≤90°. For a pure capacitor, −φ is 90°. As expected, the rates of change of −φ vs. *E* and θ vs. *E*, i.e., Δ(−φ)/Δ*E* or *d*(−φ)/*dE* and Δθ/Δ*E* or *d*θ/*dE*, are minimized at θ ≈ 0 (see Fig. 6). At the minimum lagged phase shift for the optimum intermediate frequency (1 Hz) shown in Fig. 4(h), i.e., 0.7° at 1.100 V vs. SCE, it appears that the adsorption of OH and superposition of various effects are maximized or almost saturated. In other words, θ can be set to unity. At θ ≈ 1, $(R_S + R_F)$ is much greater than $1/\omega C_P$ (see Table 1 and Fig. 3(h)). In Eqs. (4)-(6), *Z* is substantially determined by $(R_S + R_F)$, i.e., Z_{RE}, and so −φ has a minimum value of ≥0°. For a pure resistor, −φ is 0°. Similarly, the rates of change of −φ vs. *E* and θ vs. *E* are also minimized at θ ≈ 1. At θ ≈ 0.5, the rates of change of −φ vs. *E* and θ vs. *E* are maximized. At other values of θ, the rates of change of −φ vs. *E* and θ vs. *E* decrease symmetrically with *E* except the transition region (see Fig. 6).

By comparing the calculated phase shift (−φ) with the measured phase shift (−φ) shown in Table 1, one can conclude that the discussions on *Z* and −φ described in Eqs. (4)-(6), the reciprocal property and compensation of R_F and C_P in Eq. (5), and the determination of the optimum intermediate frequency (1 Hz) for the phase-shift profile (−φ vs. *E*) shown in Fig. 4 are valid and effective. Fig. 5 also shows that the determination of the optimum intermediate frequency (1 Hz) shown in Fig. 4 is reasonable.

Fig. 6 shows that the rate of change of −φ vs. *E*, i.e., Δ(−φ)/Δ*E* or *d*(−φ)/*dE*, corresponds to that of θ vs. *E*, i.e., Δθ/Δ*E* or *d*θ/*dE*, and vice versa. The rates of change of −φ vs. *E* and θ vs. *E* for the adsorption of OH are maximized at θ ≈ 0.5, decrease symmetrically with *E* at other values of θ, and are minimized at θ ≈ 0 and 1. As previously described, it is attributed to the unique nature and combination of R_ϕ and C_ϕ attaining maximum values at θ = 0.5, decreasing symmetrically with *E* at other values of θ, approaching minimum values at θ ≈ 0 and 1, and attaining minimum values at θ = 0 and 1. Correspondingly, the fitted data shown in Fig. 6 obey a Gaussian profile. The symmetrical bell-shaped curve of Δθ/Δ*E* or *d*θ/*dE* as shown in Fig. 6 is a unique feature of the Langmuir and Frumkin adsorption isotherms (θ vs. *E*). Fig. 6 also shows the validity and effectiveness of the phase-shift method. However, note that the fluctuation of Δ(−φ)/Δ*E* and Δθ/Δ*E* beyond ca. 0.675 V vs. SCE is attributed to the transition of the adsorption of OH. This is discussed in more detail in the section on the Langmuir, Frumkin, and Temkin adsorption isotherms (θ vs. *E*).

The electrode potentials (*E*) and the corresponding phase shifts (0°≤ −φ≤ 90°) shown in Table 1 or Fig. 5 are plotted as the phase-shift profile (−φ vs. *E*) for the optimum intermediate frequency (1 Hz) shown in Fig. 7. Similarly, the electrode potentials (*E*) and the corresponding fractional surface coverages (1≥θ≥0) of OH shown in Table 1 are plotted as the Langmuir and Frumkin adsorption isotherms (θ vs. *E*) of OH shown in Fig. 8. As expected, the behaviors (−φ vs. *E*) of the phase shift (0°≤ −φ≤ 90°) for the optimum intermediate frequency (1 Hz) correspond to those (θ vs. *E*) of the fractional surface coverage (1≥θ≥0) and vice versa. Note that the behavior (θ vs. *E*) of the fractional surface coverage (1≥θ≥0) is well known as the Langmuir or the Frumkin adsorption isotherm (θ vs. *E*) (see Eq. (7) or (8)).

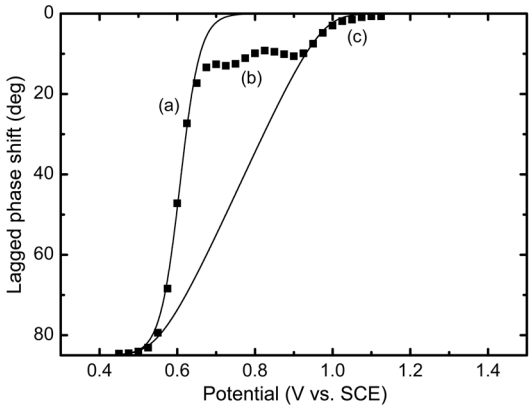

Fig. 7. Phase-shift profiles (−φ vs. E) for the optimum intermediate frequency (1 Hz) at the Pt/0.1 M KOH aqueous solution interface. (a) Region corresponding to the Langmuir adsorption isotherm (θ vs. E) of OH, (b) transition region between the Langmuir and Frumkin adsorption isotherms (θ vs. E) of OH, and (c) region corresponding to the Frumkin adsorption isotherm (θ vs. E) of OH.

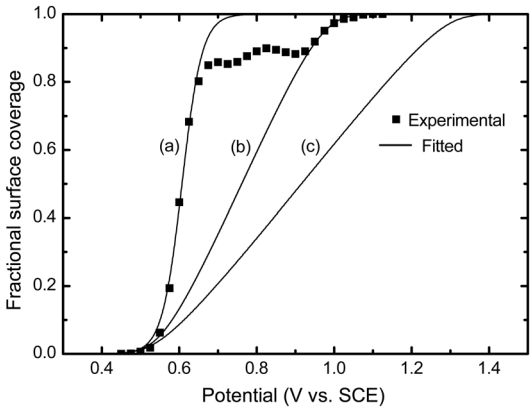

Fig. 8. Comparison of the experimental and fitted data for the Frumkin adsorption isotherms (θ vs. E) of OH at the Pt/0.1 M KOH aqueous solution interface. (a) g = 0, i.e., the Langmuir adsorption isotherm (θ vs. E), (b) g = 12, and (c) g = 24 for $K_o = 5.6 \times 10^{-10}$ mol^{-1}. Note that the Langmuir adsorption isotherm (θ vs. E), $K = 5.6 \times 10^{-10}$ mol^{-1}, shown in Fig. 8(a) is only valid at $0 \le \theta < 0.81$. The Frumkin adsorption isotherm (θ vs. E), $K = 5.6 \times 10^{-10}\exp(-12\theta)$ mol^{-1}, shown in Fig. 8(b) is only valid at $0.919 < \theta \le 1$.

3.2. The Langmuir, Frumkin, and Temkin adsorption isotherms

We consider the determination of the Langmuir, Frumkin,

and Temkin adsorption isotherms (θ vs. *E*) as follows. We determine the Langmuir adsorption isotherm (θ vs. *E*) and then find the interaction parameter (g) for the Frumkin adsorption isotherm (θ vs. *E*) based on the relevant experimental results. The applicability of the Temkin adsorption isotherm (θ vs. *E*) is considered. Finally, we derive and confirm the correlation constants between the Temkin and Langmuir or Frumkin adsorption isotherms (θ vs. *E*).

The derivation of the practical forms of the electrochemical Langmuir, Frumkin, and Temkin adsorption isotherms (θ vs. *E*) is described elsewhere.[38-40] The Langmuir adsorption isotherm (θ vs. *E*) assumes that the electrode surface is homogeneous and that the lateral interaction effect is negligible. The Langmuir adsorption isotherm (θ vs. *E*) of OH for the anodic OER can be expressed as

$$[\theta/(1-\theta)] = KC[\exp(EF/RT)], \quad (7)$$

where θ ($0 \leq \theta \leq 1$) is the fractional surface coverage of OH, K ($= k_1/k_{-1}$) is the equilibrium constant for OH,[41] C is the OH^- concentration in the bulk solution, E is the electrode potential, F is the Faraday constant, R is the gas constant, and T is the absolute temperature. In Eq. (7), E is the actual electrode potential as measured against the standard reference electrode, i.e., the SCE.

The Frumkin adsorption isotherm (θ vs. *E*) assumes that the electrode surface is inhomogeneous or that the lateral interaction effect is not negligible. The Frumkin adsorption isotherm (θ vs. *E*) of OH for the anodic OER can be expressed as follows

$$[\theta/(1-\theta)]\exp(g\theta) = K_oC[\exp(EF/RT)], \quad (8)$$

$$g = r/RT, \quad (9)$$

$$K = K_o \exp(-g\theta), \quad (10)$$

where g is the interaction parameter for the Frumkin adsorption isotherm (θ vs. *E*), K_o is the equilibrium constant for OH at g = 0, and r is the rate of change of the standard free energy of OH with θ. Note that g = 0 in Eqs. (8)-(10) is the Langmuir adsorption isotherm (θ vs. *E*) described in Eq. (7).

For the Pt/0.1 M KOH aqueous solution interface (pOH 1.01, i.e., pH 12.99), the fitted data, i.e., the numerically calculated Frumkin adsorption isotherms (θ vs. *E*) using Eq. (8), are shown in Fig. 8. Figs. 8(a), (b), and (c) show the three numerically calculated Frumkin adsorption isotherms (θ vs. *E*) corresponding to g = 0, 12, and 24 for $K_o = 5.6\times10^{-10}$ mol^{-1}, respectively. Note that g = 0 for $K_o = 5.6\times10^{-10}$ mol^{-1}, i.e., $K = 5.6\times10^{-10}$ mol^{-1}, shown in Fig. 8(a) is the Langmuir adsorption isotherm (θ vs. *E*) described in Eq. (7). The Langmuir and Frumkin adsorption isotherms (θ vs. *E*) shown in Fig. 8 can be linearly related to the phase-shift profiles (–φ vs. *E*) for the optimum intermediate frequency (1 Hz) shown in Fig. 7. From Figs. 8(a) and (b), one infers that $K = 5.6\times10^{-10}$ mol^{-1} for the Langmuir adsorption isotherm (θ vs. *E*) and $K = 5.6\times10^{-10}\exp(-12\theta)$ mol^{-1} for the Frumkin adsorption isotherm (θ vs. *E*) are applicable to the formation of OH at $0 \leq \theta < 0.81$ and $0.919 < \theta \leq 1$, respectively. Figs. 8(a) and (b) show that the adsorption of OH transits from the Langmuir to the Frumkin adsorption isotherm (θ vs. *E*), and vice versa, depending on the electrode potential (*E*). This implies that the lateral interaction effect of OH on the Pt electrode surface should be considered at $E > 0.950$ V vs. SCE. Using Eq. (9), the rate (r) of change of the standard free energy of OH is 29.8 kJ mol^{-1} for g = 12.

At intermediate values of θ, i.e., $0.2 < \theta < 0.8$, the pre-exponential term, $[\theta/(1-\theta)]$, varies little with compared to the variation of the exponential term, $\exp(g\theta)$, described in Eq. (8). Under the approximate conditions, the Temkin adsorption isotherm (θ vs. *E*) can be simply derived from the Frumkin adsorption isotherm (θ vs. *E*). The Temkin adsorption isotherm (θ vs. *E*) of OH for the anodic OER can be expressed as follows

$$\exp(g\theta) = K_oC[\exp(EF/RT)]. \quad (11)$$

Note that Eqs. (7), (8), and (11), which describe the Langmuir, Frumkin, and Temkin adsorption isotherms (θ vs. *E*), respectively, are all the same at θ = 0.5 and g = 0. This capability is attributed to the unique nature and combination of R_ϕ and C_ϕ vs. *E*. Note that the rates of change of –φ vs. *E* and θ vs. *E* are maximized at $\theta \approx 0.5$ and decrease symmetrically with *E* at other values of θ, i.e., $0.2 < \theta < 0.8$.

Fig. 9 shows, using Eq. (11), the determination of the Temkin adsorption isotherm (θ vs. *E*) correlating with the Langmuir adsorption isotherm (θ vs. *E*) shown in Fig. 8(a). At $0.2 < \theta < 0.8$, Fig. 9(b) shows an overlapped region between the Langmuir and Temkin adsorption isotherms (θ vs. *E*). This implies that the Langmuir and Temkin adsorption isotherms (θ vs. *E*) are correlated with each other even though their adsorption conditions or processes are different. In Fig. 9(b), the equilibrium constant (K_o at g = 0) and interaction parameter (g) for the Temkin adsorption isotherm (θ vs. *E*) are 5.6×10^{-9} mol^{-1} and 4.6, i.e., $K = 5.6\times10^{-9}\exp(-4.6\theta)$ mol^{-1}, respectively. Using Eq. (9), the rate (r) of change of the standard free energy of OH is 11.4 kJ mol^{-1} for g = 4.6.

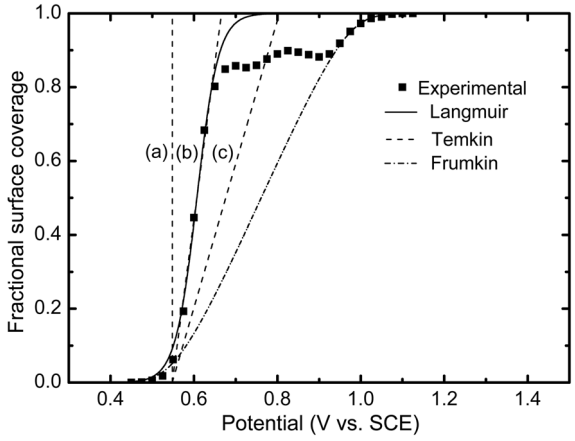

Fig. 9. Comparison of the experimental and fitted data for the Langmuir and Temkin adsorption isotherms (θ vs. E) of OH at the Pt/0.1 M KOH aqueous solution interface. (a) g = 0, (b) g = 4.6, and (c) g = 10 for $K_o = 5.6 \times 10^{-9}$ mol^{-1}. Note that the Temkin adsorption isotherm (θ vs. E), $K = 5.6\times10^{-9}\exp(-4.6\theta)$ mol^{-1}, shown in Fig. 9(b) is only valid at $0.2 < \theta < 0.8$.

3.3. Correlation constants between the Temkin and Langmuir or Frumkin adsorption isotherms

As shown in Figs. 8-10, only one adsorption isotherm (θ vs. *E*), i.e., the Langmuir or the Frumkin adsorption isotherm (θ vs. *E*), is determined based on the experimental results. Note that the Langmuir adsorption isotherms (θ vs. *E*) are always parallel to each other (see Fig. 10). This implies that the slopes of the Langmuir adsorption isotherms (θ vs. *E*) are all the same at $0.2 < \theta < 0.8$. In other words, the interaction parameters (g) for the Temkin adsorption isotherms (θ vs. *E*) correlating with the Langmuir adsorption isotherms (θ vs. *E*) are all the same. The interaction parameter (g) for the Temkin adsorption isotherm (θ vs. *E*) is consistently ca. 4.6 greater than that (g) for the correlating Langmuir adsorption isotherm (θ vs. *E*) (see Fig. 9). Note that the Langmuir and Temkin adsorption isotherms (θ vs. *E*) are correlated with each other even though their adsorption conditions or processes are different. Similarly, one can interpret that the interaction parameter (g) for the Temkin adsorption isotherm (θ vs. *E*) is consistently ca. 4.6 greater than that (g) for the correlating Frumkin adsorption isotherm (θ vs. *E*). Because the Frumkin adsorption isotherm (θ vs. *E*) is determined referred to the Langmuir adsorption isotherm (θ vs. *E*), i.e., g = 0 (see Figs. 8 and 9). As previously described, this capability is attributed to the unique nature and combination of R_ϕ and C_ϕ vs. *E*. The rates of change of –φ vs. *E* and θ vs. *E* are maximized at $\theta \approx 0.5$ and decrease symmetrically with *E* at other values of θ, i.e., $0.2 < \theta < 0.8$. In addition, one can confirm that the equilibrium constant (K_o) for the Temkin adsorption isotherm (θ vs. *E*) is ca. 10 times greater than that (K or K_o) for the Langmuir or the Frumkin adsorption isotherm (θ vs. *E*) (see Fig. 9). These numbers (ca. 10 times and 4.6) can be taken as correlation constants between the Temkin and Langmuir or Frumkin adsorption isotherms (θ vs. *E*).[23,25,26,30] Consequently, one can interpret that the Temkin adsorption isotherm (θ vs. *E*) correlating with the Langmuir or the Frumkin adsorption isotherm (θ vs. *E*), and vice versa, is readily determined using the correlation constants. The two different adsorption isotherms (θ vs. *E*), i.e., the Temkin and Langmuir or Frumkin adsorption isotherms (θ vs. *E*), can appear to fit the same data at $0.2 < \theta < 0.8$.

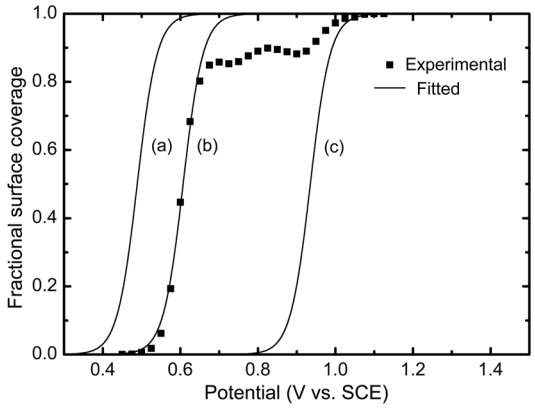

Fig. 10. Comparison of three numerically calculated Langmuir adsorption isotherms (θ vs. E) of OH at the Pt/0.1 M KOH aqueous solution interface. (a) $K = 5.6 \times 10^{-8}$ mol^{-1}, (b) $K = 5.6 \times 10^{-10}$ mol^{-1}, and (c) $K = 1.6 \times 10^{-15}$ mol^{-1}.

3.4. Standard free energy of adsorption

The standard free energy of OH is given by the difference between the standard molar Gibbs free energy of OH and that of a number of water molecules on the adsorption sites of the Pt electrode surface. Under the Langmuir adsorption conditions, the relation between the equilibrium constant (K) and the standard free energy (ΔG_{ads}^0) of OH is given as follows[38,42,43]

$$2.3RT \log K = -\Delta G_{ads}^0 \quad (12)$$

Under the Frumkin adsorption conditions, the relation between the equilibrium constant (K) and the standard free energy (ΔG_θ^0) of OH is given as follows

$$2.3RT \log K = -\Delta G_\theta^0 \quad (13)$$

In contrast to ΔG_{ads}^0 described in Eq. (12), ΔG_θ^0 depends on θ, i.e., $0 \le \theta \le 1$. The standard free energies (ΔG_{ads}^0, ΔG_θ^0) of OH and the equilibrium constants (K) for the Langmuir, Temkin, and Frumkin adsorption isotherms (θ vs. *E*) of OH are summarized in Table 2. As expected, the adsorption of OH is an endothermic reaction, i.e., ΔG_{ads}^0 and $\Delta G_\theta^0 > 0$.

4. Conclusions

The phase-shift method and correlation constants, i.e., the electrochemical impedance spectroscopy (EIS) techniques for studying linear relationships between the behaviors (–φ vs. *E*) of the phase shift ($0^o \le -\varphi \le 90^o$) for the optimum intermediate frequency and those (θ vs. *E*) of the fractional surface coverage

Table 2. Comparison of the standard free energies (ΔG_{ads}^0, ΔG_θ^0) of OH and the equilibrium constants (K) for the Langmuir, Temkin, and Frumkin adsorption isotherms (θ vs. *E*) of OH at the Pt/0.1 M KOH aqueous solution interface.

Adsorption isotherm	ΔG_{ads}^0, ΔG_θ^0 (kJ mol^{-1})	K (mol^{-1})	θ
Langmuir [a]	$\Delta G_{ads}^0 = 52.8$	5.6×10^{-10}	$0 \le \theta < 0.81$
Temkin [b]	$49.4 < \Delta G_\theta^0 < 56.2$	$2.2 \times 10^{-9} > K > 1.4 \times 10^{-10}$	$0.2 < \theta < 0.8$
Frumkin [c]	$80.1 < \Delta G_\theta^0 \le 82.5$	$9.1 \times 10^{-15} > K \ge 3.4 \times 10^{-15}$	$0.919 < \theta \le 1$

[a] $K_o = 5.6 \times 10^{-10}$ mol^{-1} and g = 0, i.e., $K = 5.6 \times 10^{-10}$ mol^{-1}. At $0 \le \theta < 0.81$, the inhomogeneous and lateral interaction effects on the adsorption of OH are negligible.
[b] $K_o = 5.6 \times 10^{-9}$ mol^{-1} and g = 4.6, i.e., $K = 5.6 \times 10^{-9}\exp(-4.6\theta)$ mol^{-1}. The Temkin adsorption isotherm (θ vs. *E*) is only valid at $0.2 < \theta < 0.8$ (see Fig. 9).
[c] $K_o = 5.6 \times 10^{-10}$ mol^{-1} and g = 12, i.e., $K = 5.6 \times 10^{-10}\exp(-12\theta)$ mol^{-1}. At $0.919 < \theta \le 1$, the inhomogeneous or the lateral interaction effect on the adsorption of OH is not negligible.

($1 \geq \theta \geq 0$), have been proposed and verified to determine the Langmuir, Frumkin, and Temkin adsorption isotherms (θ vs. E) of H for the cathodic HER at noble and transition-metal/aqueous solution interfaces. The linear relationships between $-\varphi$ vs. E and θ vs. E have been experimentally verified based on the rates of change of $-\varphi$ vs. E and θ vs. E maximizing at $\theta \approx 0.5$, decreasing symmetrically with E at other values of θ, and minimizing at $\theta \approx 0$ and 1. This is attributed to the unique nature and combination of the faradaic resistance (R_ϕ) and adsorption pseudocapacitance (C_ϕ) attaining maximum values at $\theta = 0.5$, decreasing symmetrically with E at other values of θ, approaching minimum values at $\theta \approx 0$ and 1, and attaining minimum values at $\theta = 0$ and 1. At the Pt/0.1 M KOH aqueous solution interface, the Langmuir, Frumkin, and Temkin adsorption isotherms (θ vs. E), equilibrium constants ($K = 5.6\times 10^{-10}$ mol^{-1} at $0 \leq \theta < 0.81$, $K = 5.6\times 10^{-9}\exp(-4.6\theta)$ mol^{-1} at $0.2 < \theta < 0.8$, and $K = 5.6\times 10^{-10}\exp(-12\theta)$ mol^{-1} at $0.919 < \theta \leq 1$), interaction parameters (g = 4.6 for the Temkin and g = 12 for the Frumkin adsorption isotherm), rates of change of the standard free energy (r = 11.4 kJ mol^{-1} for g = 4.6 and r = 29.8 kJ mol^{-1} for g = 12), and standard free energies (ΔG_{ads}^0 = 52.8 kJ mol^{-1} at $0 \leq \theta < 0.81$, $49.4 < \Delta G_\theta^0 < 56.2$ kJ mol^{-1} at $0.2 < \theta < 0.8$, and $80.1 < \Delta G_\theta^0 \leq 82.5$ kJ mol^{-1} at $0.919 < \theta \leq 1$) of OH for the anodic OER are also determined using the phase-shift method and correlation constants. The adsorption of OH transits from the Langmuir to the Frumkin adsorption isotherm (θ vs. E), and vice versa, depending on the electrode potential (E) or the fractional surface coverage (θ). At $0 \leq \theta < 0.81$, the inhomogeneous and lateral interaction effects on the adsorption of OH are negligible. At $0.919 < \theta \leq 1$, the inhomogeneous or the lateral interaction effect on the adsorption of OH is not negligible. At $0.2 < \theta < 0.8$, the Temkin adsorption isotherm (θ vs. E) correlating with the Langmuir or the Frumkin adsorption isotherm (θ vs. E), and vice versa, is readily determined using the correlation constants. The phase-shift method and correlation constants are accurate and reliable techniques to determine the adsorption isotherms and related electrode kinetic and thermodynamic parameters. They are useful and effective ways to study the adsorptions of intermediates (H, OH) for the sequential reactions (HER, OER) at the interfaces.

Acknowledgements

This work was supported by the Research Grant of Kwangwoon University in 2006.

References

1. E. Gileadi (Ed.), Electrosorption, Plenum Press, New York, 1967.
2. E. Gileadi, E. Kirowa-Eisner, J. Penciner, Interfacial electrochemistry, Addison-Wesley Pub. Co. Reading, MA, 1975.
3. E. Gileadi, Electrode kinetics, VCH, New York, 1993.
4. J. O'M. Bockris, S. U. M. Khan, Surface electrochemistry, Plenum Press, New York, 1993.
5. B. E. Conway, G. Jerkiewicz (Eds.), Electrochemistry and materials science of cathodic hydrogen absorption and adsorption, PV 94-21, The Electrochemical Society, Pennington, NJ, 1995.
6. G. Jerkiewicz, Hydrogen sorption at/in electrodes, *Prog. Surf. Sci*., **57**, 137 (1998).
7. J. O'M. Bockris, A. K. N. Reddy, M. Gamboa-Aldeco, Modern electrochemistry, 2nd Ed., Vol. 2A, Kluwer Academic/Plenum Press, New York, 2000.
8. G. Jerkiewicz, J. M. Feliu, B. N. Popov (Eds.), Hydrogen at surface and interfaces, PV 2000-16, The Electrochemical Society, Pennington, NJ, 2000.
9. J. H. Chun, K. H. Ra, The phase-shift method for the Frumkin adsorption isotherms at the Pd/H_2SO_4 and KOH solution interfaces, *J. Electrochem. Soc*., **145**, 3794 (1998).
10. J. H. Chun, K. H. Ra, Hydrogen at surface and interfaces, in: G. Jerkiewicz, J. M. Feliu, B. N. Popov (Eds.), PV 2000-16, pp. 159-173, The Electrochemical Society, Pennington, NJ, 2000.
11. J. H. Chun, K. H. Ra, N. Y. Kim, The Langmuir adsorption isotherms of electroadsorbed hydrogens for the cathodic hydrogen evolution reactions at the Pt(100)/H_2SO_4 and LiOH aqueous solution interfaces, *Int. J. Hydrogen Energy*, **26**, 941 (2001).
12. J. H. Chun, S. K. Jeon, J. H. Lee, The phase-shift method for the Langmuir adsorption isotherms of electroadsorbed H for the cathodic H_2 evolution reactions at the poly-Pt electrode interfaces, *J. Korean Electrochem. Soc*., **5**, 131 (2002).
13. J. H. Chun, K. H. Ra, N. Y. Kim, Qualitative analysis of the Frumkin adsorption isotherm of the over-potentially deposited hydrogen at the poly-Ni/KOH aqueous solution interface using the phase-shift method, *J. Electrochem. Soc*., **149**, E325 (2002).
14. J. H. Chun, K. H. Ra, N. Y. Kim, Langmuir adsorption isotherms of over-potentially deposited hydrogen at poly-Au and Rh/H_2SO_4 aqueous solution interfaces: Qualitative analysis using the phase-shift method, *J. Electrochem. Soc*., **150**, E207 (2003).
15. J. H. Chun, K. H. Ra, N. Y. Kim, Abstracts of the 203rd Electrochemical Society (ECS) Meeting, Vol. 2003-01, Abstract 1270, April 27-May 2, The Electrochemical Society, Paris, France, 2003.
16. J. H. Chun, S. K. Jeon, N. Y. Kim, Abstracts of the 203rd Electrochemical Society (ECS) Meeting, Vol. 2003-01, Abstract 2332, The Electrochemical Society, April 27-May 2, Paris, France, 2003.
17. J. H. Chun, S. K. Jeon, Determination of the equilibrium constant and standard free energy of the over-potentially deposited hydrogen for the cathodic H_2 evolution reaction at the Pt-Rh alloy electrode interface using the phase-shift method, *Int. J. Hydrogen Energy*, **28**, 1333 (2003).
18. J. H. Chun, Methods for estimating adsorption isotherms in electrochemical systems, *U. S. Patent*, **6613218** (2003).
19. J. H. Chun, N. Y. Kim, Hydrogen treatment of materials. Proceedings of the 4th international conference: HTM-2004, pp. 387-393, International Scientific Committee on Hydrogen Treatment of Materials (HTM), May 17-21, Donetsk-Svyatogorsk, Ukraine, 2004.
20. J. H. Chun, S. K. Jeon, J. Y. Chun, Constant correlation factors between Temkin and Langmuir or Frumkin adsorption isotherms in electrochemical systems, *J. Korean Electrochem. Soc*., **7**, 194 (2004).
21. J. H. Chun, S. K. Jeon, B. K. Kim, J. Y. Chun, Determination of the Langmuir adsorption isotherms of under- and over-potentially deposited hydrogen for the cathodic H_2 evolution reaction at poly-Ir/aqueous solution interfaces using the phase-shift method, *Int. J. Hydrogen Energy*, **30**, 247 (2005).
22. J. H. Chun, S. K. Jeon, K. H. Ra, J. Y. Chun, The phase-shift method for determining Langmuir adsorption isotherms of over-potentially deposited hydrogen for the cathodic H_2 evolution reaction at poly-Re/aqueous solution interfaces, *Int. J. Hydrogen Energy*, **30**, 485 (2005).
23. J. H. Chun, S. K. Jeon, N. Y. Kim, J. Y. Chun, The phase-shift method for determining Langmuir and Temkin adsorption isotherms of over-potentially deposited hydrogen for the cathodic H_2 evolution reaction at the poly-Pt/H_2SO_4 aqueous solution interface, *Int. J. Hydrogen Energy*, **30**, 1423 (2005).

24. J. H. Chun, N. Y. Kim, The phase-shift method for determining adsorption isotherms of hydrogen in electrochemical systems, *Int. J. Hydrogen Energy*, **31**, 277 (2006).
25. J. H. Chun, S. K. Jeon, J. Y. Chun, Determination of the Langmuir and Temkin adsorption isotherms of H for the cathodic H_2 evolution reaction at a Pt/KOH solution interface using the phase-shift method, *J. Korean Electrochem. Soc.*, **9**, 19 (2006).
26. J. H. Chun, S. K. Jeon, J. Y. Chun, The phase-shift method and correlation constants for determining adsorption isotherms of hydrogen at a palladium electrode interface, *Int. J. Hydrogen Energy*, **32**, 1982 (2007).
27. K. Kvastek, V. Horvat-Radosevic, Comment on the paper 'Langmuir adsorption isotherms of over-potentially deposited hydrogen at poly-Au and Rh/H_2SO_4 aqueous solution interfaces : Qualitative analysis using the phase-shift method', *J. Electrochem. Soc.*, **151**, L9 (2004).
28. A. Lasia, Comments on 'The phase-shift method for determining Langmuir adsorption isotherms of over-potentially deposited hydrogen for the cathodic H_2 evolution reaction at poly-Re/aqueous solution interfaces. Hydrogen Energy, 30 (2005) 485-499', *Int. J. Hydrogen Energy*, **30**, 913 (2005).
29. J. H. Chun, K. H. Ra, N. Y. Kim, Response to comment on 'Langmuir adsorption isotherms of over-potentially deposited hydrogen at poly-Au and Rh/H_2SO_4 aqueous solution interfaces: Qualitative analysis using the phase-shift method', *J. Electrochem. Soc.*, **151**, L11 (2004).
30. J. H. Chun, S. K. Jeon, N. Y. Kim, J. Y. Chun, Response to comments on 'The phase-shift method for determining Langmuir adsorption isotherms of over-potentially deposited hydrogen for the cathodic H_2 evolution reaction at poly-Re/aqueous solution interfaces. Hydrogen Energy, 30 (2005) 485-99', *Int. J. Hydrogen Energy*, **30**, 919 (2005).
31. M. R Tarasevich, A. Sadkowski, E. Yeager, in Comprehensive treatise of electrochemistry, B. E. Conway, J. O' M. Bockris, E. Yeager, S. U. M. Khan, R. E. White, Editors, Vol. 7, pp. 301-398, Plenum Press, New York (1983).
32. E. Gileadi, Electrode kinetics, pp. 172-177, VCH, New York, 1993.
33. J. O'M. Bockris, S. U. M. Khan, Surface electrochemistry, pp. 344-345, Plenum Press, New York, 1993.
34. E. Gileadi, E. Kirowa-Eisner, J. Penciner, Interfacial electrochemistry, pp. 6, 72-73, Addison-Wesley Pub. Co. Reading, MA, 1975.
35. E. Gileadi, E. Kirowa-Eisner, J. Penciner, Interfacial electrochemistry, pp. 86-93, Addison-Wesley Pub. Co. Reading, MA, 1975.
36. E. Gileadi, Electrode kinetics, pp. 293-303, VCH, New York, 1993.
37. E. Barsoukov, J. R. Macdonald, Eds., Impedance spectroscopy, 2nd Ed., pp. 489-493, Wiley-Interscience, New York, 2005.
38. E. Gileadi, Electrode kinetics, pp. 261-280, VCH, New York, 1993.
39. J. O'M. Bockris, S. U. M. Khan, Surface electrochemistry, pp. 280-283, Plenum Press, New York, 1993.
40. J. O'M. Bockris, A. K. N. Reddy, M. Gamboa-Aldeco, Modern electrochemistry, 2nd Ed., Vol. 2A, pp. 1193-1194, Kluwer Academic/ Plenum Pub. Co. New York, 2000.
41. D. W. Oxtoby, H. P. Gillis, N. H. Nachtrieb, Principles of modern chemistry, 5th Ed., p. 446, Thomson Learning Inc. 2002.
42. E. Gileadi, Electrosorption, pp. 1-18, in : E. Gileadi (Ed.), Plenum Press, New York, 1967.
43. E. Gileadi, Electrode kinetics, pp. 307-318, VCH, New York, 1993.